Linear-response study of plasmon excitation in metallic thin films: Layer-dependent hybridization and dispersion

Zhe Yuan[1,3] and Shiwu Gao[2,3]
[1]*Department of Applied Physics, Chalmers University of Technology, SE-412 96, Göteborg, Sweden*
[2]*Department of Physics, Göteborg University, SE-412 96 Göteborg, Sweden*
[3]*Institute of Physics, Chinese Academy of Sciences, 100080 Beijing, China*
(Received 20 December 2005; published 10 April 2006)

We present a theoretical study of collective plasmon excitation in metal thin films using the jellium model. The excitation spectra are calculated in the linear response theory and the time-dependent local density approximation. The evolution from surface plasmons at large thickness to the hybridized thin film plasmons at smaller thickness is obtained as functions of atomic layers and electron momenta. The energies of the hybridized plasmons follow qualitatively the classical electrodynamical model at large to intermediate thickness. For ultrathin films with a few atomic layers, these plasmon resonances evolve into intraband and interband transitions at small momenta. The latter results from the quantized electron states normal to the films.

DOI: 10.1103/PhysRevB.73.155411 PACS number(s): 78.66.−w, 73.20.Mf, 71.45.Gm

I. INTRODUCTION

Collective electronic excitation of solid surfaces plays a central role in many surface dynamical phenomena and processes. Excitation of surface plasmons accompanies large electron density oscillations localized near the surface. Such localized oscillations are sensitive not only to the geometric and electronic structure at surfaces, but also to the dynamical processes occurring in the surface region. It is the common ground for surface sensitivity in many spectroscopies. During the past two decades, surface plasmons have been intensively investigated by both theory[1,2] and experiment.[3–7] Experimental studies of surface plasmons have focused on the excitation energies and dispersions, which are accessible by a number of spectroscopic techniques such as electron energy loss spectroscopy (EELS),[3] optical absorption and transmission,[4] photoemission and inverse photoemission,[5] and surface enhanced Raman spectroscopy (SERS).[6] Theoretical understanding on surface plasmons has been based on either classical models[8–11] or quantum-mechanical calculations.[12–17] Linear response theory combined with time-dependent local density approximation[18,19] (TDLDA) provides one of the most accurate approaches to surface plasmons. It has been successfully applied to describe the plasmon energies and dispersions of metal surfaces,[15–17] adsorbed overlayers,[20] semiconductor quantum wells, and thin films.[21,22] In atomic and molecular systems, TDLDA has also been very successful in the description of plasmon excitations for atoms,[18,19] molecules,[23] and small metal clusters.[24,25]

The aim of this work is to explore the collective plasmon excitation of metal thin films, whose thickness can be controlled continuously layer by layer. This work is motivated by the recent experimental progress in the preparation and characterization of high quality thin films using molecular beam epitaxy (MBE).[26] The precise control of the film thickness down to single atomic layer offers the unique possibility to engineer electronic states normal to the film. How such layer-resolved thin films modulate their physical and chemical properties has received much attention in recent experiments. So far, quantum oscillations have been observed in the superconducting transition temperature,[27] electron-phonon coupling,[28] work functions,[5,28] the critical magnetic field for superconductivity,[29] and catalytic reactions in the Pb and Pt films on a Si(111) 7×7 substrate.[30] These oscillations, which were obtained as a function of atomic layers, are attributable to the quantization of electronic states normal to the surface. In a recent experiment, plasmon excitation of silver thin films on the Si(111) 7×7 substrate has also been measured as a function of film thickness.[31]

Qualitatively, thin film plasmons can be understood in a one-dimensional model by solving the classical Maxwell equations.[8] The coupling between the surface plasmons at two sides of the film results in hybridization between the two surface modes. It leads to two coupled modes $\omega_{\pm}$ of the thin film

$$\omega_{\pm}(q,D) = \frac{\omega_p}{\sqrt{2}}(1 \pm e^{-qD})^{1/2}. \quad (1)$$

Here ω_p is the bulk plasmon frequency. The energy splitting between the two modes depends on the film thickness D and the parallel momentum q. The low-energy mode ω_- corresponds to a symmetric induced charge distribution across the film (breathing mode), while the high-energy mode ω_+ has an antisymmetric charge distribution (sloshing mode). In the thick-film limit, the coupling between the two surfaces of the film becomes weak. The thin film plasmons reduce to two degenerate surface plasmons, whose frequency equals $\omega_p/\sqrt{2}$. The classical model in Eq. (1) gives an approximate description of the energy splitting of thin film plasmons.

One of the common drawbacks of the classical models is the ignorance of the electronic structures of bulk materials and at surfaces. This drawback is in sharp contrast with the observation that surface plasmons are extremely sensitive to the ground state electronic structure at a surface and its dynamical response to external perturbations. Using the hydrodynamic model, Bennett first demonstrated the dependence

of plasmon dispersion on the electron density profile at surfaces.[9] Later, Schwartz and Schaich carried out a more detailed analysis with different model electron densities and boundary conditions, and concluded that both the frequency and the dispersion of the surface plasmons sensitively depend on the surface electronic distribution.[10] These model studies demonstrated the importance of the microscopic electronic structures in the description of plasmon excitations.

On a more quantitative level, surface plasmons of metal thin films and semiconductor quantum wells have been investigated quantum mechanically. Using a jellium model, Eguiluz[13] first applied the random phase approximation (RPA) to calculate the electronic excitation of metal thin films based on the self-consistent electronic structure of the jellium slabs obtained by Lang and Kohn. This approach was pursued further by Dobson and Schaich,[21,22] who studied the excitation spectra of neutral and charged slabs at small wave vectors within TDLDA. The two coupled plasmon modes $\omega_{\pm}$ of a thin film were found in the calculated spectra. Moreover, there was an additional peak near $0.8\omega_p$. It was not clear from their calculation whether this mode corresponds to collective electron oscillation or intersubband transitions.[22] Recently, Leseduarte *et al.*[32] carried out a semiclassical calculation for the collective excitation in metal slabs within RPA. The dispersion of the high-energy modes obtained by this model is different from that of Dobson and Schaich for the same film. In the small q limit, ω_+ approaches $0.8\omega_p$, while the multipole plasmon mode[16,17] is close to ω_p. All these previous studies only calculated a few arbitrarily chosen thicknesses, and did not yield layer-resolved information in the excitation spectra in detail.

In this work, we report on a systematic TDLDA study of the collective plasmon excitation of metal thin films, focusing on their layer-dependent splitting and dispersion. The film thickness has been continuously scanned from a few tenth nanometers to a single atomic layer. As the thickness decreases, the evolution from surface plasmons to hybridized thin film plasmons is obtained as functions of film thickness and wave vector. At large and intermediate thickness, the energy splitting between the thin film plasmons follows qualitatively the classical electrodynamic model. For ultrathin films with a few atomic layers, transition from plasmon excitations to intraband and interband electron-hole pair excitations has been observed at small momenta. Comparison between the classical model and the quantum-mechanical calculations is also made. Quantum effects in the plasmon dispersion, the intersubband transitions, and the multipole plasmon excitation are found at small wave vectors and in the thin-film limit.

The rest of this paper is organized as follows. In Sec. II, the computational methods are outlined. In Sec. III, the results of a thick slab are first compared with those given by Lang and Kohn and Liebsch for a semi-infinite jellium surface. It is followed by a systematic study of thin film plasmons. The validity and limitation of the classical models are discussed. Finally in Sec. IV, we give a short summary of this paper.

II. THEORETICAL METHODS

Following the early works on surface[2,17] and thin film plasmons,[13,21,22] we developed a self-consistent density functional approach for the ground state electronic structure and a linear response scheme for excitation properties. In this section, various ingredients involved in our calculations are detailed below.

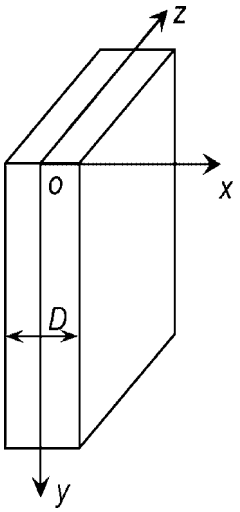

FIG. 1. Schematic illustration of the jellium slab with thickness D used in the calculation.

A. Electronic structure of a jellium thin film

We used a jellium model and the self-consistent density functional theory (DFT) approach[33,34] to describe the electronic structure of the thin films. In the jellium model, the ion charges are approximated by a uniform positive background as follows:

$$n_{\text{ion}} = \begin{cases} n_0, & |x| \leq D/2, \\ 0, & |x| > D/2. \end{cases} \tag{2}$$

Here D is the thickness of the film (see Fig. 1). The valence electrons of the jellium are described by two equivalent parameters, the electron density n_0 or the average electron radius r_s

$$n_0 = \frac{3}{4\pi r_s^3}. \tag{3}$$

Due to the translational symmetry and homogeneity parallel to the surface, the y-z plane, the effective one-electron potential depends only on the coordinate normal to the film x. The wave functions and eigenenergies of the system can be written in the following forms (atomic units are used in this paper $e=m=\hbar=1$):

$$\Psi_{n,\vec{k}_{\parallel}} = e^{i\vec{k}_{\parallel}\cdot\vec{r}_{\parallel}}\psi_n(x), \tag{4}$$

$$E_{n,\vec{k}_{\parallel}} = \varepsilon_n + \frac{1}{2}|\vec{k}_{\parallel}|^2. \tag{5}$$

Here $\vec{k}_{\parallel}$ and $\vec{r}_{\parallel}$ are the parallel components of the electron momentum and position vector, respectively. The normal

eigenenergies $\{\varepsilon_n\}$ and wave functions $\{\psi_n\}$ fulfill the following one-dimensional Kohn-Sham equation:

$$\left[-\frac{1}{2}\frac{d^2}{dx^2}+v_{\text{eff}}(x)\right]\psi_n(x)=\varepsilon_n\psi_n(x). \tag{6}$$

The effective one-electron potential $v_{\text{eff}}(x)$ consists of two parts: the electrostatic potential φ and the exchange-correlation potential v_{xc} (Ref. 35)

$$v_{\text{eff}}(x)=\varphi(x)+v_{\text{xc}}(x). \tag{7}$$

The electrostatic potential is obtained by solving the Poisson equation and the exchange-correlation part is described by the local-density approximation (LDA) with Wigner's formula.[2] By solving Eq. (6) self-consistently, the ground state eigenenergies and wave functions of the system are obtained. The electron density for a finite slab is given by

$$n(x)=2\sum_{E_{n,\vec{k}_\parallel}<E_F}|\Psi_{n,\vec{k}_\parallel}(\vec{r})|^2=\frac{1}{\pi}\sum_{\varepsilon_n<E_F}(E_F-\varepsilon_n)|\psi_n(x)|^2. \tag{8}$$

In general, the Fermi energy of a thin film differs from that of the semi-infinite surface, especially when D is small. In our calculation, E_F is determined by the charge neutrality condition

$$\int_{-\infty}^{\infty}n(x)dx=n_0D. \tag{9}$$

Equation (6) is numerically solved on a uniform grid. The eigenenergies and wave functions are obtained by diagonalizing the Hamiltonian matrix.

B. Linear response of the jellium thin film

With the computed electronic structure, electronic excitations of the jellium slab induced by an external field can be calculated in the linear response theory, which has been adopted in early studies of surface plasmon[2,17] and thin film plasmons.[13,21,22] Here we are concerned with the excitation induced by inelastic electron scattering, as measured by EELS. The perturbation potential of the impact electrons is modeled by a charged sheet approaching the jellium slab from one side ($x>0$). It takes the following form:[36]

$$\phi_{\text{ext}}(x,q)=-\frac{2\pi}{q}e^{qx}, \tag{10}$$

where $q=|\vec{q}_\parallel|$ is the magnitude of the parallel momentum. For a weak external field, the response of the electron gas can be obtained in the linear response function as follows:[37]

$$\delta n(x,q,\omega)=\int dx'\chi(x,x',q,\omega)\phi_{\text{ext}}(x',q). \tag{11}$$

Here χ is the linear response function, and δn is the induced electron density. Within the TDLDA and the many body perturbation theory,[38] χ can be obtained perturbatively by solving the following Dyson equation:

$$\chi(x,x',q,\omega)=\chi_0(x,x',q,\omega)+\int dx_1\int dx_2\chi_0(x,x_1,q,\omega)\times K(x_1,x_2,q)\chi(x_2,x',q,\omega), \tag{12}$$

where K is the kernel of the effective electron-electron interaction. In TDLDA, the kernel for the jellium systems reads

$$K(x_1,x_2,q)=\frac{2\pi}{q}e^{-q|x_1-x_2|}+\left.\frac{\delta V_{\text{xc}}}{\delta n}\right|_{n=n(x_1)}\delta(x_1-x_2). \tag{13}$$

We also used Wigner's formula of the exchange-correlation kernel as in the ground state calculation. In Eq. (12) χ_0 is the response function of the noninteracting electrons, which is constructed from the eigenenergies and wave functions obtained from Eq. (6),[37]

$$\chi_0(x,x',q,\omega)=\int d(\vec{r}_\parallel-\vec{r}'_\parallel)e^{-i\vec{q}_\parallel\cdot(\vec{r}_\parallel-\vec{r}'_\parallel)}\tilde{\chi}_0(\vec{r},\vec{r}',\omega), \tag{14}$$

$$\tilde{\chi}_0(\vec{r},\vec{r}',\omega)=\sum_{n,\vec{k}_\parallel}\sum_{m,\vec{k}'_\parallel}\frac{f_{n,\vec{k}_\parallel}-f_{m,\vec{k}'_\parallel}}{\omega-E_{m,\vec{k}'_\parallel}+E_{n,\vec{k}_\parallel}+i\eta}\times\Psi^\star_{n,\vec{k}_\parallel}(\vec{r})\Psi_{n,\vec{k}_\parallel}(\vec{r}')\Psi_{m,\vec{k}'_\parallel}(\vec{r})\Psi^\star_{m,\vec{k}'_\parallel}(\vec{r}'), \tag{15}$$

where the Fermi-Dirac distribution function is defined as

$$f_{n,\vec{k}_\parallel}=\begin{cases}2, & \varepsilon_n+\frac{1}{2}|\vec{k}_\parallel|^2\leqslant E_F,\\ 0, & \varepsilon_n+\frac{1}{2}|\vec{k}_\parallel|^2>E_F.\end{cases} \tag{16}$$

In the numerical implementation, the response functions are represented on the same grid as that used in solving Eq. (6). Therefore $\chi_0(x,x',q,\omega)$, $K(x,x',q)$, and $\chi(x,x',q,\omega)$ are all matrices, whose rank is equal to the dimension of the grid.[39] In the evaluation of χ_0, the sum over $\vec{k}_\parallel$ in Eq. (15) can be done analytically, giving the following expression of χ_0:[13,14]

$$\chi_0(x,x',q,\omega)=\sum_{n=1}^{M}\sum_{m=1}^{\infty}F_{nm}(q,\omega)\psi^\star_n(x)\psi_n(x')\psi_m(x)\psi^\star_m(x'), \tag{17}$$

$$F_{nm}(q,\omega) = -\frac{1}{\pi q^2}\left\{ q^2 - 2(\varepsilon_n - \varepsilon_m) + i\left[2q^2(E_F - \varepsilon_n) - \left(\frac{1}{2}q^2 - \varepsilon_n + \varepsilon_m - \omega - i\eta \right)^2 \right]^{1/2} - i\left[2q^2(E_F - \varepsilon_n) - \left(\frac{1}{2}q^2 - \varepsilon_n + \varepsilon_m + \omega + i\eta \right)^2 \right]^{1/2} \right\}. \quad (18)$$

In Eq. (17), the sum over n runs over the number of occupied states M, while the sum over m runs over both the occupied and unoccupied states.

As soon as we are concerned with the asymmetric perturbation induced by the impact electrons in EELS, the surface response function can be defined as

$$g(q,\omega) = \int dx e^{qx} \delta n(x,q,\omega) = -\frac{2\pi}{q} \int dx \int dx' e^{qx} \chi(x,x',q,\omega) e^{qx'}. \quad (19)$$

The imaginary part of the surface response function $\mathrm{Im}[g(q,\omega)]$, the surface loss function, is related directly to the energy loss spectra measured by EELS.[40,41]

III. RESULTS AND DISCUSSIONS

A. Comparison between a thick film and the semi-infinite surface

Before studying thin film plasmons, we calculated a thick slab to compare with the semi-infinite jellium surface. Our calculation reproduces both the ground state and excitation properties of the jellium surface.

To simulate the Ag thin films studied in the experiment,[31] a density $r_s=3$ is chosen. Figure 2 shows the ground state electron density and the effective potential near the surface of the slab with $D=12\lambda_F$ ($\lambda_F=9.82$ a.u. is the Fermi wavelength). The results for the jellium surface[35] with $r_s=3$ are also plotted (dots) in Fig. 2. Here, the comparison is made only in the surface region, where the Friedel oscillation and quantum spill out of the electrons are significant. The electron density and effective potential obtained in our calculation are in close agreement with those given by Lang and Kohn.[35]

Figure 3 shows the surface loss function $\mathrm{Im}[g(q,\omega)]$ as a function of energy for the same slab as in Fig. 2 at three different wave vectors: $q=0.05$, 0.075, and 0.15 a.u., respectively. The plasmon dispersion is given in the inset for a wide range of momentum. Again the excitation spectra compare well with those obtained by the semi-infinite jellium surface.[42] The bulk plasmon frequency is $\omega_p=9.1$ eV, which corresponds to a surface plasmon frequency $\omega_s=\omega_p/\sqrt{2}=6.4$ eV. In Fig. 3, each curve shows a main peak close to the energy of the surface plasmon. The dispersion of these peaks is in good agreement with that obtained for the semi-infinite surface. In particular, it has a negative slope in the small q region and a positive slope at large q. Such a dispersion has been well documented for jellium metal surfaces.[1,15,43] In addition, there is a weak yet discernible peak at 7.8 eV in Fig. 3, which is characteristic for multipole plasmon excitation. The multipole mode is usually weak and can hardly be distinguishable from the tail of surface plasmon in high density metals. This is especially true at large q.[16,17]

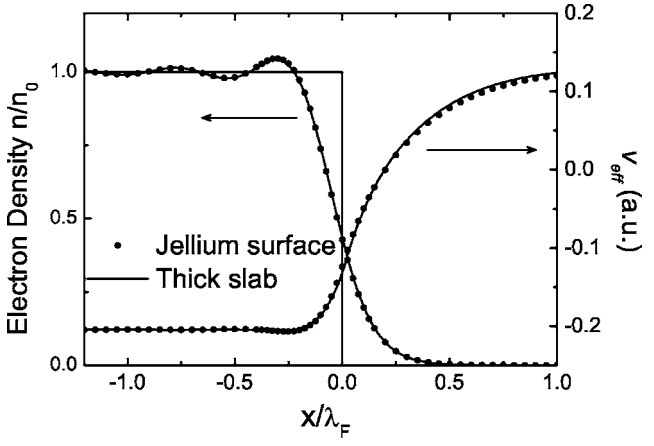

FIG. 2. The ground state electron density and the one-electron potential near the surface of a thick film with $D=12\lambda_F=117.84$ a.u. The background of positive charge has density $n_0=3/(4\pi r_s^3)=8.84\times10^{-3}$ a.u. The dots are the results by Lang and Kohn for the semi-infinite jellium surface at the same density (Ref. 35).

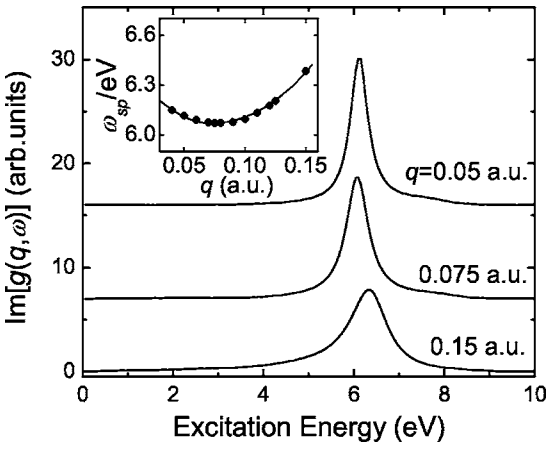

FIG. 3. Energy and momentum dependence of the surface loss function $\mathrm{Im}[g(q,\omega)]$ for the thick film with $D=12\lambda_F$ at three different q. The resonance peak in each spectrum near 6.4 eV is the surface plasmon resonance of the jellium surface. Inset: the plasmon dispersion of the metal film from our calculation (dots) compares favorably with that of the semi-infinite surface (solid curve).

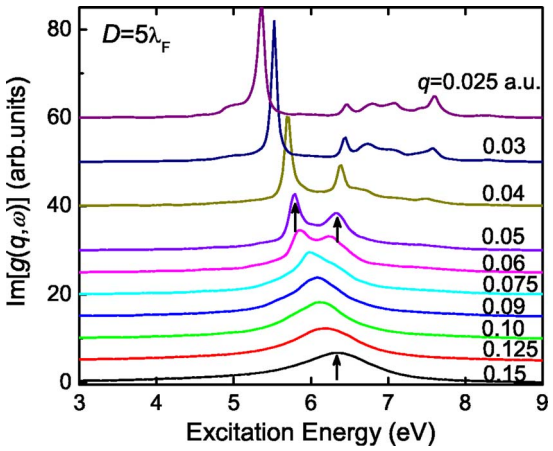

FIG. 4. (Color online) The wave vector dependence of the surface loss function $\mathrm{Im}[g(q,\omega)]$ for a thin film with $D=5\lambda_F$. The plasmon resonance peak splits at $q=0.075$ a.u. The three arrows mark the peak positions, at which the induced electron densities are shown in Fig. 5. All the curves are offset for clarity.

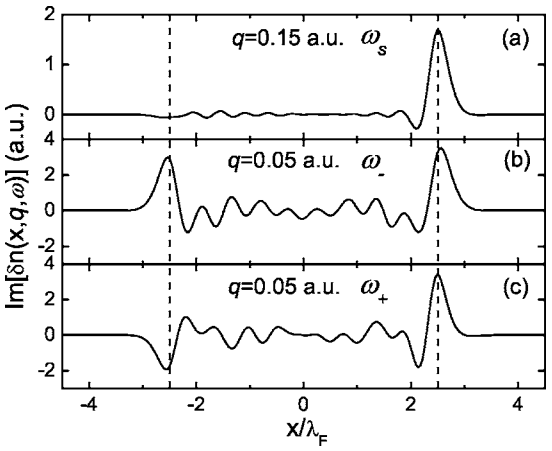

FIG. 5. The induced electron densities of the plasmon resonances marked by arrows in Fig. 4. The dashed lines show the positions of the thin film edge.

B. Thin film plasmons and their thickness dependence

The finite thickness of a thin film introduces electron confinement and quantization perpendicular to the film. In this section, the thickness dependence of the excitation properties is explored systematically as a function of atomic layers.

Figure 4 shows the surface loss function $\mathrm{Im}[g(q,\omega)]$ for a typical thin film with $D=5\lambda_F$. The excitation spectra are plotted as functions of energy and wave vector. The q dependence of the spectra is characterized by three different regions and evolves from surface plasmons to thin film plasmons. At large q, $q>0.075$ a.u., only one plasmon peak is observable in each spectrum. It corresponds to the surface plasmon at one side of the slab excited by the impact electrons. The plasmon energy has a positive dispersion as q increases as found for many metal surfaces.[17] At intermediate q, $0.04<q<0.075$ a.u., the plasmon resonance splits into two peaks, corresponding to the two hybridized modes given in Eq. (1). This splitting becomes larger as the wave vector decreases. At small q, $q<0.04$ a.u., more substructures appear in the spectrum, especially in the energy range of 7–8 eV. This feature results from the interaction of the multipole plasmon with the antisymmetric mode. It will be discussed in detail later.

Figure 5(a) shows the induced electron density of the resonance peak at $q=0.15$ a.u. marked by an arrow in Fig. 4. Here, only the electrons at the right-hand side of the slab are excited due to the external field assumed in Eq. (10). The electrons at the left-hand side of the slab do not respond to the incoming electrons, because the perturbation potential decays rapidly inside the film at large q. This is in agreement with the experimental observations that the plasmon dispersion of all thin films approaches that of the surface plasmon in the large q limit.[31] As q decreases, the external potential penetrates gradually into the film. Electrons at both surfaces of the slab start to respond to the external field and interact with each other, leading to plasmon hybridization between the two surfaces. The splitted plasmon peaks at intermediate q result from the hybridization of surface plasmons, as expected by Eq. (1). Figures 5(b) and 5(c) show the induced electron densities of the two peaks at $q=0.05$ a.u., also marked by arrows in Fig. 4. The density of the low-energy peak, Fig. 5(b), shows symmetric distribution across the slab. In contrast, the high-energy mode in Fig. 5(c) has an antisymmetric density response. This picture of plasmon hybridization is very similar to the cases in nanoshells and other nanostructures.[44–47]

We pushed our calculation further to the very small q limit in order to gain insight into the excitation properties of the thin films induced by optical excitation. It can be seen from Fig. 4 that in the small q limit, the antisymmetric mode splits into more substructures due to the coupling to the multipole plasmon excitation. The induced charge and field of the multipole mode extend much deeper into the slab and can only couple to the antisymmetric mode. The multipole modes are only observable at small wave vectors[16,17] in the energy range of $0.8\omega_p$. From Fig. 5(c), it can be seen that the antisymmetric mode has two opposite induced charge sheets at the two sides of the slab. The field of the antisymmetric mode is thus extending in the whole slab. In comparison, the density of the symmetric mode is much localized near the surface as shown in Fig. 5(b). It has thus little coupling to the multipole mode.

As the thickness of the film further decreases, the interaction between the two surface plasmon modes becomes stronger, and electron quantization normal to the surface is more prominent. These two effects lead to larger splitting between the symmetric and antisymmetric modes at large q and a more pronounced single-particle character at small q. Figure 6 shows the excitation spectrum for $D=0.5\lambda_F$, which corresponds to an ultrathin film with a single atomic layer. At large q, the two resonance peaks for the symmetric and antisymmetric mode are still observable. The splitting between them is, however, much larger compared to the case for $D=5\lambda_F$ shown in Fig. 4 at the same wave vector. At small q, the symmetric mode is greatly enhanced and its linewidth becomes much smaller. Accompanied with the enhancement of the symmetric mode, the broad antisymmetric band disap-

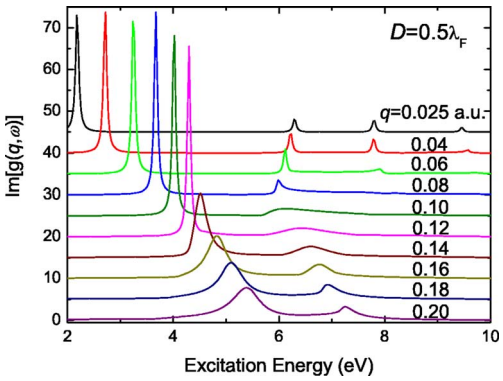

FIG. 6. (Color online) The wave vector dependence of the surface loss function $\mathrm{Im}[g(q,\omega)]$ for the thin film with $D=0.5\lambda_F$. The single particle excitations appear in the energy band of the antisymmetric mode at small q. All the curves are offset for clarity.

pears. Instead, a few discrete peaks show up. These discrete peaks correspond to electron-hole pair excitations between the discrete energy subbands in the normal direction. The q dependence of the excitation spectra shown in Fig. 6 clearly shows the transition from plasmonlike excitation to single-particle excitation in the ultrathin films.

The character of the single particle excitations in the ultrathin films can be understood qualitatively from the external potential and the electronic structure of the noninteracting jellium films. At small q, the external potential in Eq. (10) can be expanded as

$$\phi_{\mathrm{ext}}(x,q)|_{q\to 0} = -\frac{2\pi}{q} - 2\pi x + O(q). \tag{20}$$

This potential yields two different kinds of transitions according to the Fermi's golden rule. The first term in Eq. (20) gives rise to intraband transitions between states with the same inversion symmetry across the film, while the second term corresponds to interband dipole transitions between states with different symmetry. The decreasing linewidth of the intraband mode at small q results from the reduced phase space for intraband transitions.[48] The enhanced intensity indicates the collective character of this mode even in the small q limit. In contrast, the discrete peaks in the high energy band (6–10 eV) are completely single-particle-like and do not exhibit any collective behavior. Checking the sum-rule indicates that the two types of transitions have equal partial sum, due to the symmetry in the ground-state wave functions.

Figure 7 shows the dispersion and splitting of the thin film plasmons as a function of film thickness $D=12\lambda_F-3.5\lambda_F$. Here a monolayer of the closely packed Ag (111) surface corresponds to approximately $0.5\lambda_F$. The dashed line in each panel is the plasmon dispersion of the semi-infinite jellium surface.[42] At large q, the plasmon dispersions of all thin films coincide with the surface plasmon independent of the film thickness. At each thickness, a critical wave vector q_c, below which the symmetric and antisymmetric modes start to split, can be clearly seen. At very small q, more substructures appear in the antisymmetric band. Yet the spectrum is still fitted

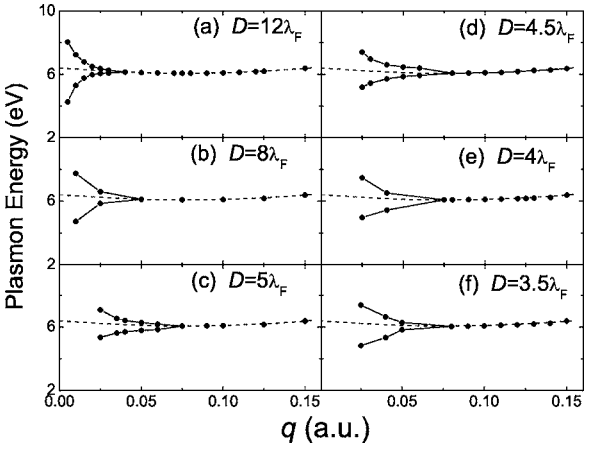

FIG. 7. The dispersion of the thin film plasmons as a function of thickness, which is varied layer by layer at small thicknesses $D<5\lambda_F$. The dashed line in each panel shows the surface plasmon dispersion for the semi-infinite jellium surface.[42]

by a single Lorentzian in the energy range covering all these substructures.[49] This fitting scheme leads to a large uncertainty in the antisymmetric mode at small q. Figure 8 shows the layer-dependent dispersions for even thinner films with $D=3\lambda_F$ to $0.5\lambda_F$. As D decreases, the splitting occurs at larger q. In addition, single particle excitations start to dominate the spectrum at small wave vectors. The plasmon dispersions in Figs. 7 and 8 show a monotonic variation with the film thickness, and does not exhibit any oscillation as observed in the work function,[5,28] superconducting transition temperature,[27] and electron-phonon coupling.[28]

Figure 9 shows the dependence of q_c on the film thickness. It increases gradually as the thickness decreases. For a thinner slab $D=2\lambda_F$, q_c is about 0.18 a.u., while it is about 0.03 a.u. for a thicker slab $D=12\lambda_F$. When the thickness approaches to infinity, q_c goes to zero. No splitting occurs in the surface plasmon. The interaction between two surfaces results from the penetration of the external field, which is dependent on the product of wave vector and the film thickness. The interaction is only noticeable when the product qD

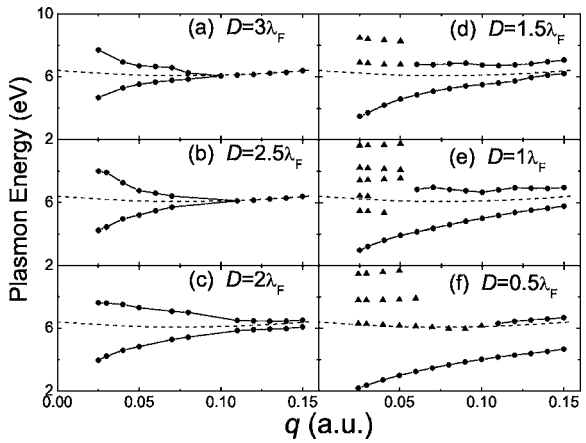

FIG. 8. The same as Fig. 7 for $D=3\lambda_F$ to $0.5\lambda_F$. For extremely thin films, the single particle transitions (triangles) appear at small q in the antisymmetric band.

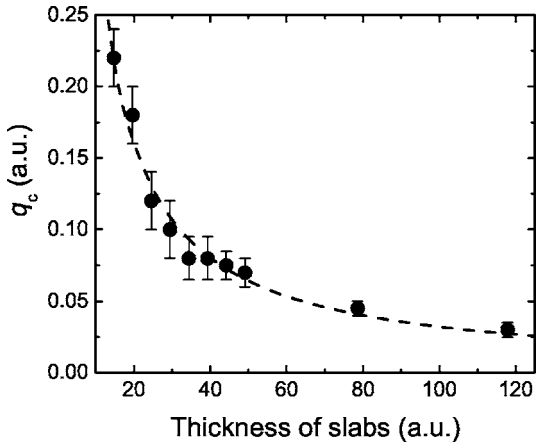

FIG. 9. The critical wave vector q_c at which the plasmon modes split, as a function of the film thickness D. The dashed line shows the curve fitted by $q_c=3.2/D$.

is small enough. Therefore, the product q_cD is nearly constant for all films calculated, as expected by the classical model in Eq. (1).

Figure 10 summarizes the energies of the symmetric and antisymmetric plasmons as a function of the film thickness at a fixed wave vector $q=0.025$ a.u. The plasmon energies calculated by Eq. (1) are also given for comparison (solid lines). Since the surface plasmon of the classical model $\omega_s=\omega_p/\sqrt{2}=6.4$ eV has no dispersion, the solid lines generally deviate from the TDLDA results, especially at large thickness. If we replace the surface plasmon frequency $\omega_p/\sqrt{2}$ in Eq. (1) with the dispersive $\omega_s(q=0.025)=6.235$ eV given by TDLDA, a better agreement can be found between TDLDA and the "dispersive" classical model. For ultrathin films, the antisymmetric band is gradually substituted by the single-particle transitions. From the thickness dependence of the critical wave vector (Fig. 9) and the energy splitting (Fig. 10) between the symmetric and antisymmetric modes, we can

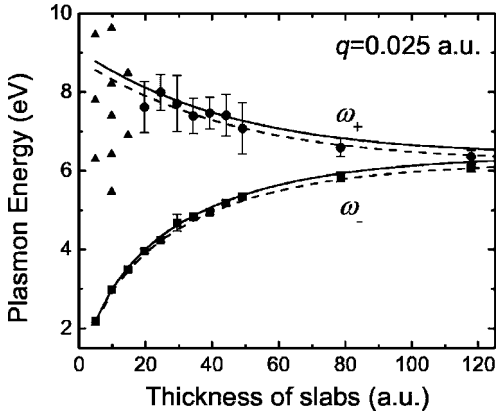

FIG. 10. The plasmon energies of the symmetric (squares) and antisymmetric modes (dots) as a function of film thicknesses at $q=0.025$ a.u. Solid lines: the energies $\omega_\pm$ are calculated by Eq. (1). Dashed lines: $\omega_\pm$ are calculated by replacing $\omega_p/\sqrt{2}=6.4$ eV with the dispersive $\omega_s(q=0.025)=6.235$ eV obtained from TDLDA. For very small thickness, the single particle excitations (triangles) appear in the antisymmetric band.

conclude that the classical model in Eq. (1) gives a fair qualitative description of the plasmon hybridization and splitting in the thick films. However, it cannot describe the quantum features of the spectra in the thin-film limit.

A detailed comparison between the jellium model and the experimental data is not yet possible so far, due to the fact that the present model neglected two aspects of the experimental system. (1) The d band of the silver film is not described in the jellium slab.[42] As a result, the plasmon energy of the jellium model is higher than the experimental value 3.9 eV. (2) In the experiment, the silver films are adsorbed on the silicon substrate, which has not been considered in the present study. Nevertheless, the general features of the collective excitation obtained by the symmetric jellium model are still meaningful for the understanding of thin film plasmons, at least on the conceptual level.

C. Quantum effects of plasmon excitation in thin films

In this section, we discuss some of the differences between the quantum mechanical model and the classical model. Such differences can be best demonstrated by a dynamical response function $d(\omega)$, which is often used in the study of surface plasmons[1,50,51]

$$d(\omega)=\frac{\int dzz\,\delta n(z,\omega)}{\int dz\,\delta n(z,\omega)}. \tag{21}$$

Here $\delta n(z,\omega)$ is the induced electron density in the linear response regime. The $d(\omega)$ function is generally complex. In the classical model, this function is simply a real delta function localized exactly at the edge of the slab, because the induced charge is determined by the sharp boundary condition in classical electrodynamics. In TDLDA, $\delta n(z,\omega)$ has a finite density distribution due to the quantum fluctuation of the electronic system as shown in Fig. 5. Although the distribution of δn is still localized in the surface region, it does not fully coincide with the jellium edge. The deviation of $d(\omega)$ from the surface edge defines the dynamical image plane, which is usually about 1 a.u. outside the jellium surface. It characterizes the dynamical response of the electrons at a metal surface.

With the fundamental difference illustrated in $d(\omega)$, many physical quantities can be expressed in terms of $d(\omega)$. Below are a few quantities relevant for thin film plasmons.

(i) In the classical model, the energy of the surface plasmon is a constant $\omega_s=\omega_p/\sqrt{2}$ and has no dispersion. In TDLDA, it has a negative dispersion at small q and a positive one at large q. The dispersion at small q can be expressed as follows:[17,43]

$$\omega_s(q)=\frac{\omega_p}{\sqrt{2}}\left[1-\frac{q}{2}d\left(\frac{\omega_p}{\sqrt{2}}\right)+O(q^2)\right]. \tag{22}$$

It can be seen that the dispersion is dependent on $d(\omega)$. Thin film plasmons, which result from the hybridization of the surface plasmons, cannot be well described by the classical

model due to the fundamental difference in $d(\omega)$. In contrast, the TDLDA calculation gives a quantitative description of the plasmon dispersion.

(ii) The quantum confinement of the electrons in the normal direction is only described in the quantum mechanical model. The quantization of the normal wave functions leads to electron-hole pair excitations between the subbands. This is especially obvious at small wave vectors, as shown in Fig. 4. For ultrathin films, the interband and intraband transitions even dominate the excitation spectrum at small q as shown in Fig. 6. Such quantum nature of electrons and its associated properties are not accounted for in any classical models.

(iii) The multipole modes of thin film plasmons cannot be accounted for by the classical model, but appear naturally in the TDLDA calculations. For semi-infinite surfaces, the surface response function is related to $d(\omega)$ in the small q limit:[1,17]

$$g(q,\omega) \approx \frac{\epsilon(\omega)-1}{\epsilon(\omega)+1}\left[1+\frac{2\epsilon(\omega)}{\epsilon(\omega)+1}qd(\omega)\right]. \qquad (23)$$

The plasmon modes are the poles of this response function.[17] The $d(\omega)$ function has a pole at around $\omega \approx 0.8\omega_p$,[50] which corresponds to the multipole resonance.[16,17] In metal thin films, the multipole plasmon also exists at large and intermediate thickness. It interacts with the antisymmetric mode ω_+ as shown in Fig. 4. This conclusion is in agreement with that found in the semiclassical approach.[32]

IV. CONCLUSIONS

We have studied the excitation spectra of metal thin films using the linear response theory and the jellium model of the electronic structures. The energies and dispersions of surface plasmons are obtained as a function of film thickness. As the thickness decreases, the excitation spectra show evolution from surface plasmons at large thickness to the hybridized thin film plasmons at intermediate thickness. They transform into single-particle excitations in ultrathin films.

The dispersion of the surface plasmons is characterized by three typical regions. (i) At large wave vectors, the dispersion of the plasmon resonance approaches that of the surface plasmon, due to the fact that this plasmon is localized at one side of the film. (ii) At intermediate wave vectors, the plasmon resonance splits into the symmetric and antisymmetric mode due to the penetration of external potential into the film. It leads to hybridization between the surface plasmons. (iii) At small wave vectors, the symmetric branch of the thin film plasmons evolves into the intraband transitions, which is still collective in character. In contrast, the antisymmetric band mixes with the multipole plasmon at intermediate thickness and transforms into single particle transitions in ultrathin films.

The classical model gives an approximate description of the interaction and energy splitting between the thin film plasmons, especially at large thickness. Yet it does not account for any quantum-mechanical features of the excitation spectra, such as the plasmon dispersion, the multipole modes, and single particle excitations. These effects result from the quantized motion of electrons in the normal direction and the dynamical response at surfaces. It would be interesting in the future to investigate how these quantum-mechanical behaviors affect other physical and chemical properties of these thin films.

ACKNOWLEDGMENTS

This work has been supported by the PhotoNano program, the material consortium-ATOMICS of the Swedish Foundation for Strategic Research (SSF), and the 100-Talent Program (Bairen Jihua) of Chinese Academy of Sciences. We thank D. S. Wang, Qikun Xue, Kehui Wu, and Enge Wang for useful communications.

[1] P. J. Feibelman, Prog. Surf. Sci. **12**, 287 (1982).
[2] A. Liebsch, *Electronic Excitations at Metal Surfaces* (Plenum, New York, 1997).
[3] M. Rocca, Surf. Sci. Rep. **22**, 1 (1995).
[4] U. Kreibig and M. Vollmer, *Optical Properties of Metal Clusters* (Springer, Berlin, 1995).
[5] T.-C. Chiang, Surf. Sci. Rep. **39**, 181 (2000).
[6] M. Moskovits, Rev. Mod. Phys. **57**, 783 (1985).
[7] P. M. Echenique, R. Berndt, E. V. Chulkov, Th. Fauster, A. Goldmann, and U. Höfer, Surf. Sci. Rep. **52**, 219 (2004).
[8] R. H. Ritchie, Phys. Rev. **106**, 874 (1957).
[9] A. J. Bennett, Phys. Rev. B **1**, 203 (1970).
[10] C. Schwartz and W. L. Schaich, Phys. Rev. B **26**, 7008 (1982).
[11] K. Dharamvir, B. Singla, K. N. Pathak, and V. V. Paranjape, Phys. Rev. B **48**, 12 330 (1993).
[12] P. J. Feibelman, Phys. Rev. B **9**, 5077 (1974).
[13] A. G. Eguiluz, Phys. Rev. Lett. **51**, 1907 (1983).
[14] A. G. Eguiluz, Phys. Rev. B **31**, 3303 (1985).
[15] K.-D. Tsuei, E. W. Plummer, and P. J. Feibelman, Phys. Rev. Lett. **63**, 2256 (1989).
[16] K.-D. Tsuei, E. W. Plummer, A. Liebsch, K. Kempa, and P. Bakshi, Phys. Rev. Lett. **64**, 44 (1990).
[17] K.-D. Tsuei, E. W. Plummer, A. Liebsch, E. Pehlke, K. Kempa, and P. Bakshi, Surf. Sci. **247**, 302 (1991).
[18] A. Zangwill and P. Soven, Phys. Rev. A **21**, 1561 (1980).
[19] M. J. Stott and E. Zaremba, Phys. Rev. A **21**, 12 (1980).
[20] A. Liebsch, Phys. Rev. Lett. **67**, 2858 (1991).
[21] J. F. Dobson, Phys. Rev. B **46**, 10 163 (1992).
[22] W. L. Schaich and J. F. Dobson, Phys. Rev. B **49**, 14 700 (1994).
[23] Z. H. Levine and P. Soven, Phys. Rev. A **29**, 625 (1984).
[24] W. Ekardt, Phys. Rev. B **31**, 6360 (1985).
[25] D. E. Beck, Phys. Rev. B **30**, 6935 (1984).
[26] C.-S. Jiang, S.-C. Li, H.-B. Yu, D. Eom, X.-D. Wang, Ph. Ebert, J.-F. Jia, Q.-K. Xue, and C.-K. Shih, Phys. Rev. Lett. **92**, 106104 (2004).
[27] Y. Guo, Y.-F. Zhang, X.-Y. Bao, T.-Z. Han, Z. Tang, L.-X. Zhang,

W.-G. Zhu, E. G. Wang, Q. Niu, Z. Q. Qiu, J.-F. Jia, Z.-X. Zhao, and Q.-K. Xue, Science **306**, 1915 (2004).
[28] Y.-F. Zhang, J.-F. Jia, T.-Z. Han, Z. Tang, Q.-T. Shen, Y. Guo, Z. Q. Qiu, and Q.-K. Xue, Phys. Rev. Lett. **95**, 096802 (2005).
[29] X.-Y. Bao, Y.-F. Zhang, Y. Wang, J. F. Jia, Q.-K. Xue, X. C. Xie, and Z.-X. Zhao, Phys. Rev. Lett. **95**, 247005 (2005).
[30] Q.-K. Xue *et al.* (unpublished).
[31] Y. Yu, Y. Jiang, Z. Tang, Q.-L. Guo, J.-F. Jia, Q.-K. Xue, K.-H. Wu, and E.-G. Wang, Phys. Rev. B **72**, 205405 (2005).
[32] S. Leseduarte, J. Sellares, and A. Travesset, Surf. Sci. **384**, 1 (1997).
[33] P. Hohenberg and W. Kohn, Phys. Rev. **136**, B864 (1964).
[34] W. Kohn and L. J. Sham, Phys. Rev. **140**, A1133 (1965).
[35] N. D. Lang and W. Kohn, Phys. Rev. B **1**, 4555 (1970).
[36] A. Liebsch, Phys. Scr. **35**, 354 (1987).
[37] A. L. Fetter and J. D. Walecka, *Quantum Theory of Many-Body Systems* (McGraw-Hill, New York, 1971).
[38] G. Onida, L. Reining, and A. Rubio, Rev. Mod. Phys. **74**, 601 (2002).
[39] Shiwu Gao and Zhe Yuan, Phys. Rev. B **72**, 121406(R) (2005).
[40] B. N. J. Persson, Phys. Rev. Lett. **50**, 1089 (1983).
[41] B. N. J. Persson and E. Zaremba, Phys. Rev. B **31**, 1863 (1985).
[42] A. Liebsch, Phys. Rev. Lett. **71**, 145 (1993).
[43] P. J. Feibelman, Phys. Rev. B **40**, 2752 (1989).
[44] E. Prodan, C. Radloff, N. J. Halas, and P. Nordlander, Science **302**, 419 (2003).
[45] P. Nordlander, C. Oubre, E. Prodan, K. Li, and M. I. Stockman, Nano Lett. **4**, 899 (2004).
[46] P. Nordlander and E. Prodan, Nano Lett. **4**, 2209 (2004).
[47] F. Le, N. Z. Lwin, J. M. Steele, M. Käll, N. J. Halas, and P. Nordlander, Nano Lett. **5**, 2009 (2005).
[48] H. Ishida and A. Liebsch, Phys. Rev. B **54**, 14 127 (1996).
[49] E. Prodan and P. Nordlander, Nano Lett. **3**, 543 (2003).
[50] A. Liebsch, Phys. Rev. B **36**, 7378 (1987).
[51] B. N. J. Persson and P. Apell, Phys. Rev. B **27**, 6058 (1983).